Theoretical study of laser-excited Mach cones in dusty plasmas

Lu-Jing Hou* and You-Nian Wang
State Key Laboratory of Materials Modification by Beams, Department of Physics, Dalian University of Technology, Dalian 116023, China

Z. L. Mišković
Department of Applied Mathematics, University of Waterloo, Waterloo, Ontario, Canada N2L 3G1
(Received 12 May 2004; revised manuscript received 9 August 2004; published 16 November 2004)

A two-dimensional hydrodynamic model for a monolayer of dust particles is used to study the Mach cones excited by a moving laser beam through dusty plasmas. Numerical results for the density perturbation and the velocity distribution of dust particles exhibit both compressional and shear-wave Mach cones. It is found that the compressional Mach cones exist in cases of both supersonic and subsonic excitations, and that they consist of multiple lateral or transverse wakes. On the other hand, realization of single shear-wave Mach cones depends closely on the excitation technique, the laser scanning speed, and the discharge pressures. It is found that, when the scanning direction of the laser beam is perpendicular to the laser force, a transition from multiple compressional Mach cones to a single shear Mach cone can be achieved either by lowering the scanning speed or by increasing the discharge pressures.

DOI: 10.1103/PhysRevE.70.056406 PACS number(s): 52.40.Hf, 52.25.Vy, 52.35.Fp

I. INTRODUCTION

The wake effect in dusty plasmas has been an important subject of study ever since the first observation of dusty crystals [1–4]. The initial interest in the wake effect was motivated by the need to explain the formation of vertically aligned structures in three-dimensional (3D) dust crystals. The wake in such cases is produced by the ion flow passing by a charged dust particle which is statically levitating near the edge of a plasma sheath, so that an oscillatory electrostatic potential arises in a conical region downstream of the particle. As a consequence, other dust particles may be trapped in the wells of such a potential, giving rise to the wake-induced stacking of dust particles in the direction of ion flow [5–15]. However, more recently, research interest has been shifted to another form of wake in dusty plasmas, known as the Mach cone, which consists of disturbances in the dust structure excited by an agent moving at a high speed through the plasma [16–20].

The existence of a Mach cone in dusty plasmas was first theoretically predicted in 1995 by Havnes *et al.* [21] and proposed as a possible diagnostic tool for both space and laboratory dusty plasmas [21–23]. The concept of the Mach cone has attracted much attention in theoretical [22–28], experimental [16–19], and numerical [29] research ever since. The early studies were mainly concerned with the possibility of formation of 3D Mach cones in space. In particular, a significant amount of theoretical work [21,22,24–28] has been motivated by the CASSINI mission to Saturn, where it is possible to observe Mach cones caused by big boulders moving through the dust ring of Saturn. All those theories are awaiting verification by CASSINI when it reaches Saturn some time this year.

*Email address: wljhou@student.dlut.edu.cn

However, Mach cones were first observed in experiments with dusty plasmas in earth laboratories, in the form of V-shaped disturbances of two-dimensional (2D) dust crystals, caused by charged particles [16,17] or by laser beams [18–20], moving at speeds in excess of the speed of dust acoustic waves. (Although the denomination *cone* is somewhat misleading in describing such 2D structures, we adopt the term here to underline the common origin of these V shapes in 2D and cone structures in 3D.) In particular, Samsonov *et al.* [16,17] were the first to report an observation of Mach cones, induced by some large charged particles moving slightly below a monolayer of a 2D dust crystal, which appeared in the form of double V-shaped shocks, one being compressional and the other rarefactional in nature. The opening angle of the Mach cone θ was found to obey the Mach-cone-angle relation $\sin\theta = v_s/v$, with v_s being the dust acoustic speed in plasma, and v the speed of the moving particle. This rule was verified in a wide range of Mach numbers in other experiments as well.

In a subsequent development, instead of moving charged particles, Melzer *et al.* [18] employed a laser beam with the spot moving through a 2D dust crystal at a velocity $\mathbf{v}_L$ parallel to the laser radiation force $\mathbf{F}_L$, and observed compressional-wave Mach cones composed of multiple V-shaped structures. Soon after Melzer *et al.* [18], Nosenko *et al.* [19,20] excited Mach cones in a 2D dusty crystal by using a slightly different laser excitation technique where they moved the laser spot in the direction perpendicular to the radiation force, $\mathbf{F}_L \perp \mathbf{v}_L$, and observed some new structures in addition to the usual V-shaped Mach cones. Their main new observations [18] consisted of single Mach cones composed of shear waves in the $\mathbf{F}_L \perp \mathbf{v}_L$ excitation mode, whereas a mixture of such single cones and multiple compressional-wave Mach cones was excited in the $\mathbf{F}_L \parallel \mathbf{v}_L$ mode.

Theoretical accounts of the formation of Mach cones in the above experiments were given by the observers them-

selves [16–20,30] by means of molecular-dynamics (MD) simulations, where numerical results reproduced the observations very well. In addition, an analytical theory of Mach cones induced by motion of charged particles was formulated by Dubin [24], who used a linear theory of phonon response for a 2D dust crystal, and such an approach shed additional insight into the experimental observations [16,17] for such an excitation method. On the other hand, no analytical formulation of the laser-driven Mach-cone generation is available at present. In order to complement the MD accounts [18,19,29] with an analytical approach to the formation mechanisms and structural transitions of the Mach cones excited by a laser beam, we use in this paper a 2D hydrodynamic model for the dynamics of the dust distribution in the presence of a moving laser sheath through a monolayer of dust particles. Our model for the 2D dusty plasma is a simplified version of the hydrodynamic formulation of the problem of dust acoustic waves in thin dusty layers [30]. However, we pay special attention to the damping effects due to the scattering of dust particles with neutral atoms or molecules in the plasma, which were shown to give rise to the exponential decay of waves and wakes in both the case of Mach-cone generation by moving charged particles [24] and in the wake formation by ion flow [15]. The two laser excitation techniques based on moving the laser spot parallel and perpendicular to the laser force are simulated in our model. In contrast to the previous theoretical accounts [16–20,24,29], the pure hydrodynamic model is strictly applicable to a weakly coupled dusty plasma. In order to extend our results and conclusions to the strongly coupled plasmas, in which the dust usually forms a 2D crystal structure, we take into account the correlation interactions among these dust particles semianalytically in our model. However, we find that even without considering the correlation interactions among these particles, the results belong to a "reasonable approximation"[24] for the Mach-cone formation in 2D dust crystals. The difference becomes significant only when the scanning speed is very slow. This is due to the fact that in all these observations, the typical sizes of Mach cones in strongly coupled plasmas contain several tens of the dust-lattice constants, so that a continuum limit may provide a reasonable approximation to some extent. Our numerical results are specifically designed to show the structural transition of Mach cones when the scanning speed of the laser beam and the discharge pressure change.

The outline of the paper is as follows. Basic theory is given in Sec. II, whereas the results of the numerical computations for the two excitation methods are given in Sec. III. Concluding remarks are presented in Sec. IV.

II. BASIC THEORY

In the present paper, we employ a fluid description of a monolayer of dust particles levitating in a plasma, without considering the details of interactions among dust particles. Assume that a 2D dust fluid occupies the plane $z=0$ in a Cartesian coordinate system with $\mathbf{R}=\{x,y,z\}$, and that this fluid is immersed in a large volume of plasma with the bulk values of the electron and ion number densities (assuming singly charged ions for simplicity) given by $n_{e\infty}$ and $n_{i\infty}$. Bulk conditions are reached for such distances from the dust layer that $|z| \gg \lambda_D$ (Debye screening length), and we assume that the plasma is neutral there, $n_{e\infty}=n_{i\infty}=n_0$. Let $\sigma_d(\mathbf{r},t)$ and $\mathbf{u}_d(\mathbf{r},t)$ be, respectively, the surface number density and the velocity field (having only x and y components) of the dust fluid at the position $\mathbf{r}=\{x,y\}$ and at time t. The continuity equation and the momentum equation for the fluid are, respectively,

$$\frac{\partial \sigma_d(\mathbf{r},t)}{\partial t} + \boldsymbol{\nabla}_{\parallel} \cdot [\sigma_d(\mathbf{r},t)\mathbf{u}_d(\mathbf{r},t)] = 0, \tag{1}$$

$$\frac{\partial \mathbf{u}_d(\mathbf{r},t)}{\partial t} + \mathbf{u}_d(\mathbf{r},t) \cdot \boldsymbol{\nabla}_{\parallel}\mathbf{u}_d(\mathbf{r},t) = \frac{eZ_d}{m_d}\boldsymbol{\nabla}_{\parallel}\Phi|(\mathbf{R},t)|_{z=0} + \frac{\mathbf{F}_{int}}{m_d} + \frac{\mathbf{F}_L}{m_d} - \gamma \mathbf{u}_d(\mathbf{r},t), \tag{2}$$

where m_d is mass of a dust particle, $e>0$ is the elementary charge, Z_d is the average number of excess electrons on each dust particle, and γ is the Epstein drag coefficient due to the collisions of dust particles with neutral atoms/molecules in the plasma [31]. The spatial differentiation in Eqs. (1) and (2) only includes tangential directions, viz., $\boldsymbol{\nabla}_{\parallel}=\hat{\mathbf{x}}(\partial/\partial x)+\hat{\mathbf{y}}(\partial/\partial y)$. Note that $\mathbf{F}_L(\mathbf{r},t)$ is the laser force (having only x and y components) on each dust particle, corresponding to the situation where a sheath of laser light scans through the 2D dust fluid. $\mathbf{F}_{int}$ is the internal interaction forces among the dust cloud, coming from the correlation interaction effect. It can be expressed as

$$\mathbf{F}_{int} = -\boldsymbol{\nabla}_{\parallel}\left(\frac{\delta G}{\delta \sigma_d}\right) \tag{3}$$

with $G[\sigma_d]=\int d\mathbf{r}\sigma_d(\mathbf{r},t)\varepsilon_c[\sigma_d]$ being the function of correlation energy $\varepsilon_c[\sigma_d]$ in the dust cloud.

The first term on the right-hand side of Eq. (2) indicates that, although the total electrostatic potential $\Phi(\mathbf{R},t)$ depends on all three spatial coordinates $\mathbf{R}\equiv\{\mathbf{r},z\}$, only the x and y components of the electrostatic force, evaluated in the plane $z=0$, affect the motion of the dust fluid. The full spatial dependence of the electrostatic potential Φ is determined by the Poisson equation in 3D,

$$\boldsymbol{\nabla}^2\Phi(\mathbf{R},t) = -4\pi e[n_i(\mathbf{R},t) - n_e(\mathbf{R},t) - Z_d\sigma_d(\mathbf{r},t)\delta(z)], \tag{4}$$

where $\boldsymbol{\nabla}=\boldsymbol{\nabla}_{\parallel}+\hat{\mathbf{z}}(\partial/\partial z)$. The electron and ion volume densities are given by the Boltzmann relations $n_e=n_0\exp(e\Phi/T_e)$ and $n_i=n_0\exp(-e\Phi/T_i)$, owing to the fact that both the movement of the laser spot and the dynamics of the massive dust particles are so slow that both electrons and ions are considered to have enough time to reach their respective local equilibria, with $T_{i\ (e)}$ being the ion (electron) temperature (we set the Boltzmann constant $k_B=1$).

In the unperturbed state of the system, we have $\mathbf{F}_L=\mathbf{0}$, $\partial/\partial t=0$, $\sigma_d\equiv\sigma_{d0}=\text{const}$, $\mathbf{u_d}\equiv\mathbf{u}_{d0}=\mathbf{0}$, $n_e\equiv n_{e0}(z)\approx n_0+n_0(e/T_e)\Phi_0(z)$, and $n_i\equiv n_{i0}(z)\approx n_0-n_0(e/T_i)\Phi_0(z)$, while the unperturbed value of the potential $\Phi_0(z)$ is determined

from the limiting form of Eq. (4), as follows:

$$\frac{d^2}{dz^2}\Phi_0 - \lambda_D^{-2}\Phi_0 = 4\pi e Z_d \sigma_{d0}\delta(z), \tag{5}$$

where $\lambda_D^{-2}=4\pi n_0 e^2[(1/T_e)+(1/T_e)]$ is the Debye length. Taking the natural boundary conditions for Φ_0 at $z=0$ [continuity of Φ_0 and $\Phi_0'(0+)-\Phi_0'(0-)=4\pi e Z_d\sigma_{d0}$], we obtain from Eq. (5)

$$\Phi_0(z) = -2\pi e Z_d \lambda_D \sigma_{d0}\exp(-|z|/\lambda_D), \tag{6}$$

and note that this solution maintains overall neutrality of the system plasma plus 2D dust fluid, viz.,

$$Z_d\sigma_{d0} = \int_{-\infty}^{\infty} dz[n_{i0}(z) - n_{e0}(z)], \tag{7}$$

under the condition $|\Phi_0| \ll T_{e,i}/e$.

In the perturbed situation, assuming a first-order perturbation in $\mathbf{F}_L$, we write $\Phi(\mathbf{R},t)=\Phi_0(z)+\Phi_1(\mathbf{R},t)$, $\sigma_d(\mathbf{r},t)=\sigma_{d0}+\sigma_{d1}(\mathbf{r},t)$, $\mathbf{u}_d(\mathbf{r},t)\equiv\mathbf{u}_{d1}(\mathbf{r},t)$, $n_e(\mathbf{R},t)=n_{e0}(z)+n_0(e/T_e)\Phi_1(\mathbf{R},t)$, and $n_i(\mathbf{R},t)=n_{i0}(z)-n_0(e/T_i)\Phi_1(\mathbf{R},t)$. Linearization of Eqs. (1)–(4) gives, respectively,

$$\frac{\partial\sigma_{d1}(\mathbf{r},t)}{\partial t} + \sigma_{d0}\nabla_\parallel\cdot\mathbf{u}_{d1}(\mathbf{r},t) = 0, \tag{8}$$

$$\frac{\partial\mathbf{u}_{d1}(\mathbf{r},t)}{\partial t} = \frac{eZ_d}{m_d}\nabla_\parallel\Phi_1(\mathbf{R},t)\big|_{z=0} + \frac{\mathbf{F}_{int}}{m_d} + \frac{\mathbf{F}_L}{m_d} - \gamma\mathbf{u}_{d1}(\mathbf{r},t), \tag{9}$$

$$\mathbf{F}_{int} = -\frac{\alpha m_d}{\sigma_{d0}}\nabla_\parallel\sigma_{d1}, \tag{10}$$

where

$$\alpha = \frac{\sigma_{d0}}{m_d}\frac{\partial^2}{\partial\sigma_{d0}^2}[\sigma_{d0}\varepsilon_c(\sigma_{d0})] \tag{11}$$

and

$$\nabla^2\Phi_1(\mathbf{R},t) = \lambda_D^{-2}\Phi_1(\mathbf{R},t) + 4\pi e Z_d\sigma_{d1}(\mathbf{r},t)\delta(z), \tag{12}$$

where we have used Eq. (4) to obtain Eq. (12). Now, we need to determine the expression of the density of the correlation energy $\varepsilon_c[\sigma_{d0}]$, so that α in Eq. (11) can be determined consequently. This is given by a numerically fitted formula [32] $\varepsilon_c[\sigma_{d0}]=(0.9851-1.0952\Gamma)T_d$, where T_d is the temperature of the dust particles and Γ is the coupling parameter given by $\Gamma=Z_d^2e^2/dT_d$, with $d=(\pi\sigma_{d0})^{-1/2}$ the Wigner-Seitz radius. Note here that the adoption of the above formula of $\varepsilon_c[\sigma_{d0}]$ implicitly requires $d/\lambda_D \ll 1$ [32]. This condition is satisfied in this paper by adjusting the experimental parameters [16–20] in a reasonable range, as will be shown in the following part. Then by subsituting $\varepsilon_c[\sigma_{d0}]$ back into Eq. (12), we get a very simple expression for α, namely $\alpha=-0.821(Z_d^2e^2/m_dd)$.

Now by using a partial Fourier transform with respect to the $\mathbf{r}$ and t dependences, we can write, e.g.,

$$\Phi_1(\mathbf{R},t) \equiv \Phi_1(\mathbf{r},z,t) = \int\frac{d^2\mathbf{k}}{(2\pi)^2}e^{i\mathbf{k}\cdot\mathbf{r}}\int\frac{d\omega}{2\pi}e^{-i\omega t}\Phi_1(\mathbf{k},z,\omega), \tag{13}$$

where $\mathbf{k}=\{k_x,k_y\}$. This allows us to reduce Eq. (12) to

$$\frac{\partial^2}{\partial z^2}\Phi_1(\mathbf{k},z,\omega) - (k^2\lambda_D^2+1)\lambda_D^{-2}\Phi_1(\mathbf{k},z,\omega) = 4\pi e Z_d\sigma_{d1}(\mathbf{k},\omega)\delta(z), \tag{14}$$

where $k^2=k_x^2+k_y^2$, which is easily solved in an analogy to the solution of Eq. (5), as follows:

$$\Phi_1(\mathbf{k},z,\omega) = -\frac{2\pi e Z_d\lambda_D}{\sqrt{k^2\lambda_D^2+1}}\sigma_{d1}(\mathbf{k},\omega)\times\exp(-\sqrt{k^2\lambda_D^2+1}|z|/\lambda_D). \tag{15}$$

After performing a Fourier transform of Eqs. (8) and (9) and elimination of the fluid velocity field, one can use Eq. (15) to express the Fourier transform of the perturbed dust-fluid surface density in terms of the Fourier transform of the laser force, as follows:

$$\sigma_{d1}(\mathbf{k},\omega) = i\frac{\sigma_{d0}}{m_d}\times\frac{\mathbf{k}\cdot\mathbf{F}_L(\mathbf{k},\omega)}{\omega(\omega+i\gamma)-\alpha k^2-\omega_{pd}^2k^2\lambda_D^2/\sqrt{k^2\lambda_D^2+1}}, \tag{16}$$

where

$$\omega_{pd} = \sqrt{\frac{2\pi e^2Z_d^2\sigma_{d0}}{m_d\lambda_D}} \tag{17}$$

is defined as the plasma frequency of a 2D dust fluid in the background plasma. Interestingly, we obtain from Eq. (16) the dispersion relation for acoustic waves in 2D dust fluid as follows:

$$\omega^2 = \frac{\omega_{pd}^2k^2\lambda_D^2}{(k^2\lambda_D^2+1)^{1/2}} - \alpha k^2, \tag{18}$$

in analogy to that of a 3D case [25,26]. Note here that Eq. (18) coincides with the semianalytic results for a 2D triangular Yukawa lattice obtained previously by Dubin [24] [with only a slight difference in the factor before the second term on the right-hand side of Eq. (18)]. Additionally, if $\alpha\rightarrow 0$, the result reduces to the case of a pure fluid description of dusty plasma, i.e., without considering the correlation effects between dust particles, and again coincides with the mean-field approximation of a 2D triangular Yukawa lattice in Ref. [24]. As for the effect of the parameter α, it is found in our later simulation that the results are not very sensitive to the variation of α.

However, here it should be pointed out that the hydrodynamic model we are using is only applicable in the long-wavelength approximation. For more advanced analysis of

this problem, one needs to adopt a more sophisticated approach, for example the quasilocalized charge approximation (QLCA) for the Yukawa liquid [33].

Furthermore, we obtain the phase speed of the long-wavelength dust acoustic waves propagating in the dust plane as $v_s=\omega/k\approx\lambda_D\sqrt{\omega_{pd}^2-\alpha/\lambda_D^2}$. Or we can have a further approximation $v_s\approx\lambda_D\omega_{pd}$, considering the fact that $1\gg\alpha/\omega_{pd}^2\lambda_D^2\approx0.26$ in our condition. This also explains why the parameter α has little effect on the simulation results. Finally, we obtain

$$\sigma_{d1}(\mathbf{r},t)=i\frac{\sigma_{d0}}{m_d}\int\frac{d^2\mathbf{k}}{(2\pi)^2}e^{i\mathbf{k}\cdot\mathbf{r}}\int_{-\infty}^{\infty}\frac{d\omega}{2\pi}e^{-i\omega t}\times\frac{\mathbf{k}\cdot\mathbf{F}_L(\mathbf{k},\omega)}{\omega(\omega+i\gamma)\varepsilon(k,\omega)},\tag{19}$$

where $\varepsilon(k,\omega)$ is the dielectric function of the present model for dusty plasma,

$$\varepsilon(k,\omega)=1-\frac{\alpha k^2+\omega_d^2}{\omega(\omega+i\gamma)},\tag{20}$$

with $\omega_d^2=\omega_{pd}^2k^2\lambda_D^2/\sqrt{k^2\lambda_D^2+1}$.

In a similar way, we obtain the Fourier transform of the perturbed velocity field of the dust fluid in terms of the Fourier transform of the laser force, as follows:

$$\mathbf{u}_{d1}(\mathbf{k},\omega)=\frac{i}{\omega+i\gamma}\frac{1}{m_d}\{\mathbf{F}_L(\mathbf{k},\omega)+[\varepsilon^{-1}(k,\omega)-1]\times\hat{\mathbf{k}}\hat{\mathbf{k}}\cdot\mathbf{F}_L(\mathbf{k},\omega)\},\tag{21}$$

with $\hat{\mathbf{k}}$ being the unit vector in the direction of $\mathbf{k}$, whereas the expression for $\mathbf{u}_{d1}(\mathbf{r},t)$ follows in analogy to Eq. (19).

For the profile of the laser force spot $\mathbf{F}_L(\mathbf{r},t)$, we adopt the elliptical Gaussian form which was proposed in Refs. [18–20]. Assuming that $\mathbf{F}_L$ acts in the x direction, and that the spot moves in the x, y plane with velocity $\mathbf{v}_L=\{v_x,v_y\}$, we can write

$$\mathbf{F}_L(\mathbf{r},t)=f_0\exp\left[-\frac{(x-v_xt)^2}{a^2}-\frac{(y-v_yt)^2}{b^2}\right]\hat{\mathbf{x}},\tag{22}$$

where f_0 is the intensity of the force and a and b are empirical parameters [18–20] defining the widths of the spot in the x and y directions, respectively. Therefore, the Fourier transform of the laser force profile in the x, y plane is given by

$$\mathbf{F}_L(\mathbf{k},\omega)=2\pi^2abf_0\delta(\omega-\mathbf{k}\cdot\mathbf{v}_L)\exp\left(-\frac{a^2}{4}k_x^2-\frac{b^2}{4}k_y^2\right)\hat{\mathbf{x}}.\tag{23}$$

In order to simulate the laser scanning technique where the laser spot moves at the speed v_L, in a direction parallel to the radiation force, $\mathbf{v}_L\|\mathbf{F}_L$, we simply set $v_x=v_L$ and $v_y=0$, whereas in the case when scanning velocity $\mathbf{v}_L$ is to be chosen perpendicular to the laser force, $\mathbf{v}_L\perp\mathbf{F}_L$, we set $v_y=v_L$ and $v_x=0$ [18–20].

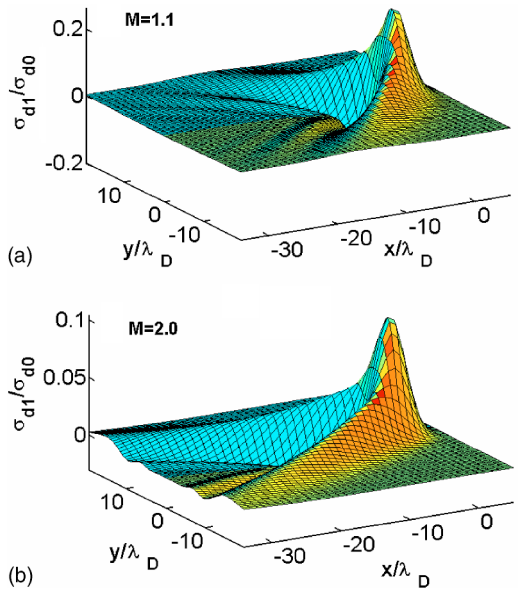

FIG. 1. The distribution of perturbed density σ_{d1} in the Mach cone region in the case of $\mathbf{v}_L\|\mathbf{F}_L$ for (a) $M=1.1$ and (b) $M=2.0$ and with discharge pressure kept at 5.0 Pa.

III. NUMERICAL RESULTS

The main parameters used in our numerical computations are all selected in accordance with the recent Mach cone experiments in dusty plasmas [16–20]. The base values of the parameters are given as follows. The bulk plasma density, $n_0=1\times10^9$ cm^{-3}; ion temperature and dust temperature, $T_i=T_d=0.03$ eV; electron temperature, $T_e=3$ eV; the mass density and the radius of dust particles, $\rho_d=1.5$ g/cm^3 and $r_d=5.0$ μm (so that $m_d\approx1.2\times10^{-13}$ g); the excess charge on each dust particle, $Z_d=5000$ (which we assume constant, for simplicity); and the surface number density of the dust fluid, $\sigma_{d0}=400$ cm^{-2}. Under these conditions, the coupling coefficient $\Gamma\approx4253$, the Debye length is $\lambda_D\approx430$ μm, and the dust plasma frequency $\omega_{pd}\approx33$ s^{-1}. The parameters in the expression for laser force are $a=b=0.1$ cm and $f_0=5.0\times10^{-13}$ dyn. Finally, the scanning speed of the laser beam v_L, given in terms of Mach number $M=v_L/v_s$, and the discharge pressure p (which determines the damping constant γ) are used as variable parameters.

A. Case $\mathbf{v}_L\|\mathbf{F}_L$

We first consider the dependence of the Mach cone structures on the scanning speed of the laser beam. Figure 1 shows the results for density perturbation σ_{d1} in a Mach cone for $M=1.1$ and $M=2.0$, with the discharge pressure kept fixed at 5.0 Pa. V-shaped Mach cones, along with multiple oscillatory lateral wakes, can be clearly identified in this figure. Several features are obvious. First, it can be seen that these structures are composed of multiple cones, with the outermost one being the most pronounced. According to an earlier theory [24] of Mach cones in dusty plasmas, these multiple structures appear to be a consequence of the strongly dispersive nature of the dust acoustic waves. Secondly, these Mach cones are composed of compressional

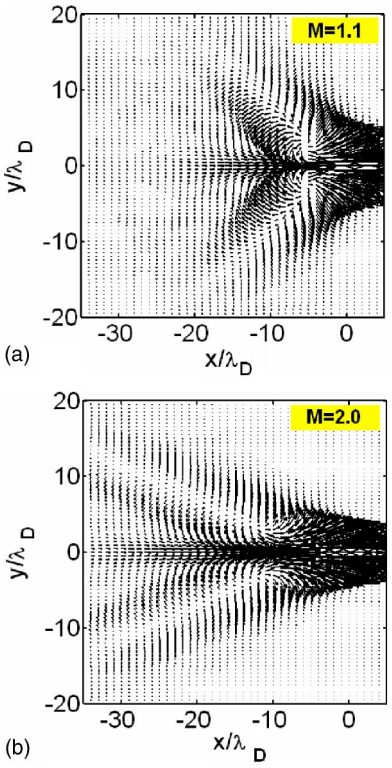

FIG. 2. The map of dust velocity field $\mathbf{u}_{d1}$ in the Mach cone region in the case of $\mathbf{v}_L \| \mathbf{F}_L$ for (a) $M=1.1$ and (b) $M=2.0$ and with discharge pressure kept at 5.0 Pa.

waves, which can be more clearly observed in the map of the dust velocity field $\mathbf{u}_{d1}$, shown in Fig. 2 for the same Mach numbers and the same pressure as in Fig. 1. In this figure, one can see that the direction of the dust particle motion is perpendicular to the cone wings and parallel to the wave propagation direction, which indicates that these Mach cones are in fact compressional waves. Furthermore, the cone opening angle roughly obeys the Mach-cone-angle relation, and it can be seen from both figures that, with a decrease in the scanning speed of the laser beam, both the opening angles and the amplitudes of the Mach cones increase monotonically. Moreover, there is an interesting feature that, if the scanning speed is further decreased, a transition from the V-shaped Mach cones to a transverse oscillatory wake can be observed. This transition is clearly shown in Fig. 3, which displays the perturbed density σ_{d1} for $M=0.6$ and $M=0.7$, with the discharge pressure kept at 2.0 Pa. Similar effects have been predicted theoretically by Dubin [24], and realized experimentally by Nosenko *et al.* recently [20]. However, we have found that these transverse waves are evident only if the discharge pressure is low enough to prevent damping due to the friction on neutral particles.

In order to illustrate the damping effect due to the neutral friction, we further vary the discharge pressure. It is found that the oscillations in the Mach cones decay very quickly as the discharge pressure increases. This is clearly seen in Figs. 4 and 5, which display, respectively, the perturbed density and the fluid velocity in the Mach cone region. In these figures, the scanning velocity is kept fixed at $M=1.1$, while the pressures are chosen to be 2.0 Pa and 10 Pa in both figures.

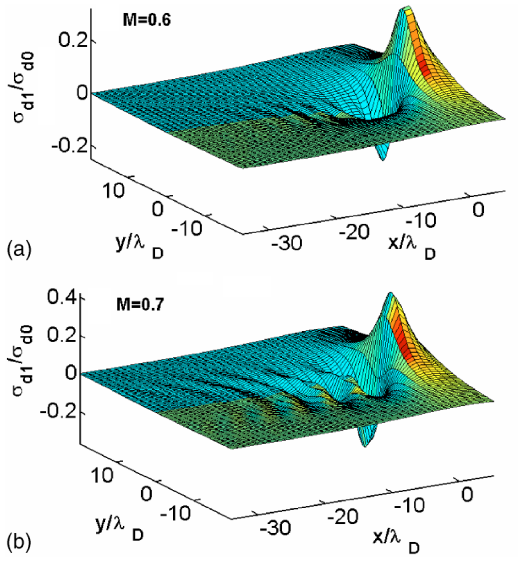

FIG. 3. The distribution of perturbed density σ_{d1} in the Mach cone region in the case of $\mathbf{v}_L \| \mathbf{F}_L$ for (a) $M=0.6$ and (b) $M=0.7$ and with discharge pressure kept at 2.0 Pa.

It is seen that damping at high pressures may appear to have the effect of reducing the number of multiple Mach cones down to two or even one. It will turn out, as shown in the following subsection, that the damping effects may have a more profound influence on the Mach cones excited by a laser beam with $\mathbf{v}_L \perp \mathbf{F}_L$.

B. Case $\mathbf{v}_L \perp \mathbf{F}_L$

We begin with the discussion of the influence of scanning speed on Mach cones. Figure 6 shows the density perturba-

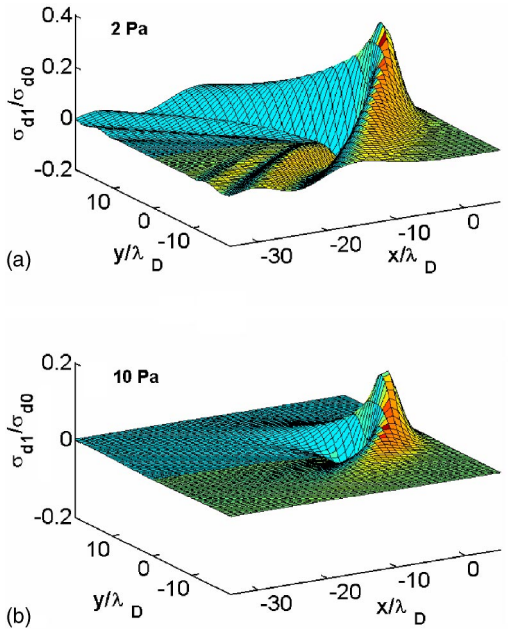

FIG. 4. The distribution of perturbed density σ_{d1} in the Mach cone region in the case of $\mathbf{v}_L \| \mathbf{F}_L$ for discharge pressures (a) $p=2.0$ Pa and (b) $p=10$ Pa and with scanning speed kept at $M=1.1$.

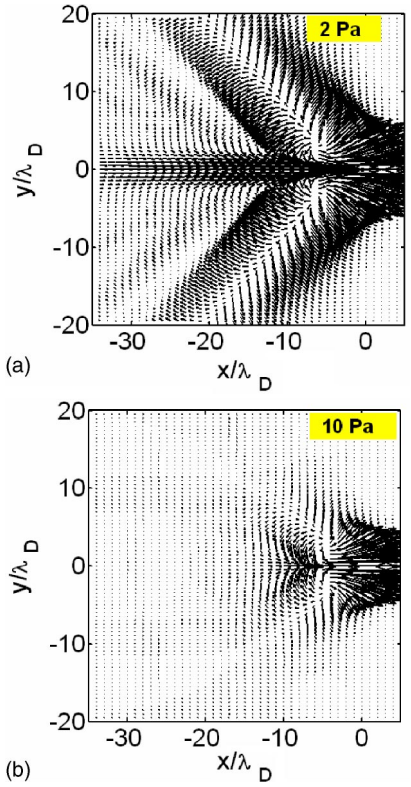

FIG. 5. The map of dust velocity field $\mathbf{u}_{d1}$ in the Mach cone region in the case of $\mathbf{v}_L \| \mathbf{F}_L$ for discharge pressures (a) $p=2.0$ Pa and (b) $p=10$ Pa and with scanning speed kept at $M=1.1$.

tion of the dust fluid σ_{d1} for $M=1.1$ and $M=2.0$, with the discharge pressure kept at 5.0 Pa. In addition to the multiple V-shaped structures of the Mach cone, seen previously in the case of $\mathbf{v}_L \| \mathbf{F}_L$, a new feature is observed. It is obvious that the density distributions are quite asymmetric, as a result of the asymmetry in the excitation technique. This tendency is more clearly exhibited in Fig. 7, showing the maps of the

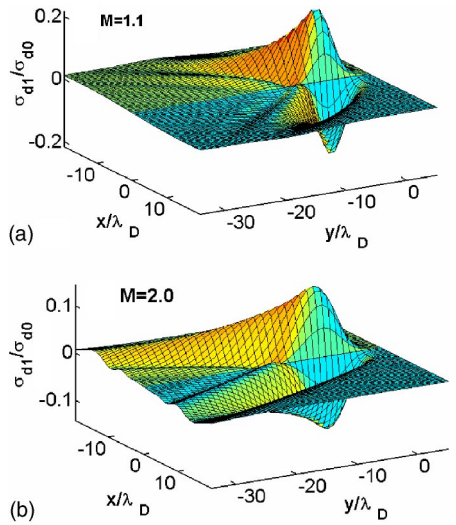

FIG. 6. The distribution of perturbed density σ_{d1} in the Mach cone region in the case of $\mathbf{v}_L \perp \mathbf{F}_L$ for (a) $M=1.1$ and (b) $M=2.0$ and with discharge pressure kept at 5.0 Pa.

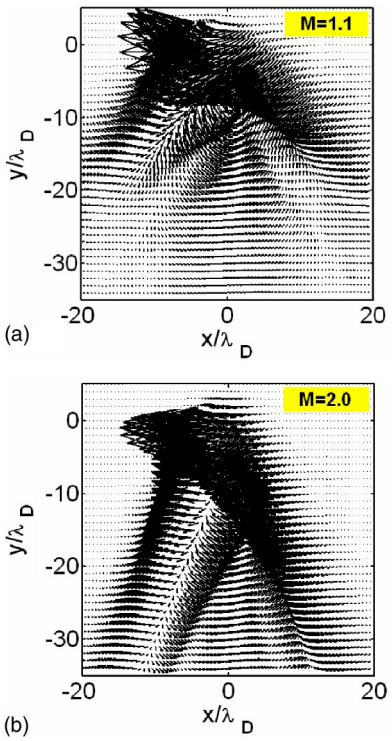

FIG. 7. The map of dust velocity field $\mathbf{u}_{d1}$ in the Mach cone region in the case of $\mathbf{v}_L \perp \mathbf{F}_L$ for (a) $M=1.1$ and (b) $M=2.0$ and with discharge pressure kept at 5.0 Pa.

velocity field $\mathbf{u}_{d1}$ in the Mach cone for the same pressure and Mach numbers as in Fig. 6. It should be noted that the multiple cones in this figure are also made of compressional waves, owing to relatively high scanning speeds. These results reproduce those of the recent experiment [20] very well. Additionally, our model also generates single-cone shear-wave [19,20] Mach cones as the scanning speed decreases. In Fig. 8, one can observe a development of single shear-wave Mach cones for speeds of $M=0.7$ and 0.8 a and pressure of 5.0 Pa. The Mach cones shown in Fig. 8 exhibit typical features of shear waves, where the particle velocity is parallel to the cone wings and perpendicular to the propagation direction of the wave, which in turn is perpendicular to the cone wings. In fact, by comparing the results in Fig. 7 with those in Fig. 8, one can clearly see a transition from multiple compressional Mach cone structures at high speeds to single shear-wave Mach cones at lower speeds. And this transition will be more significant at low pressures.

There is another way to achieve a transition between compressional and shear wave Mach cones, even when the scanning speed is relatively high. This is accomplished by increasing the discharge pressure, and hence intensifying the damping due to the neutral friction. As shown above for the $\mathbf{v}_L \| \mathbf{F}_L$ excitation mode, the oscillations within a cone are pronounced at low pressures but are efficiently damped at high pressures. This is also true here for the $\mathbf{v}_L \perp \mathbf{F}_L$ excitation mode, as seen in Fig. 9 showing the density perturbation for pressures of 2.0 Pa and 10 Pa, with the speed kept at $M=1.1$. As expected, the oscillations fade with the increase of pressure, and practically only the first cone remains at the pressure of 10 Pa in Fig. 9(b). The corresponding velocity

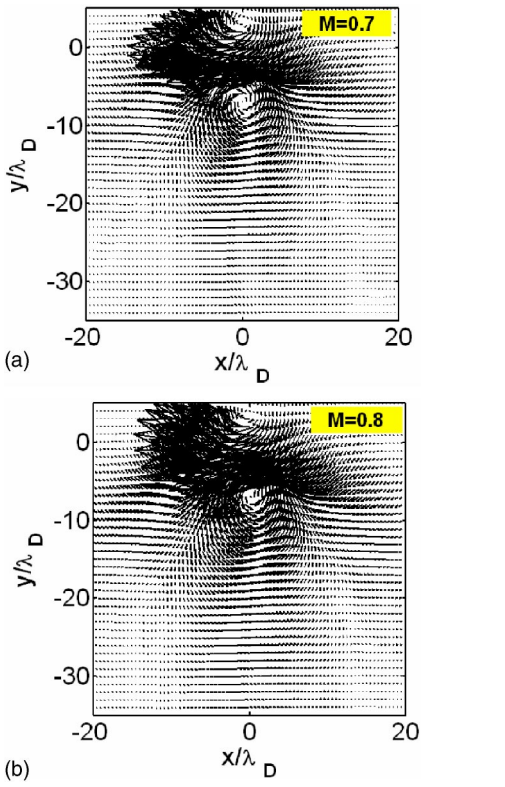

FIG. 8. The map of dust velocity field $\mathbf{u}_{d1}$ in the Mach cone region in the case of $\mathbf{v}_L \perp \mathbf{F}_L$ for (a) $M=0.7$ and (b) $M=0.8$ and with discharge pressure kept at 5.0 Pa.

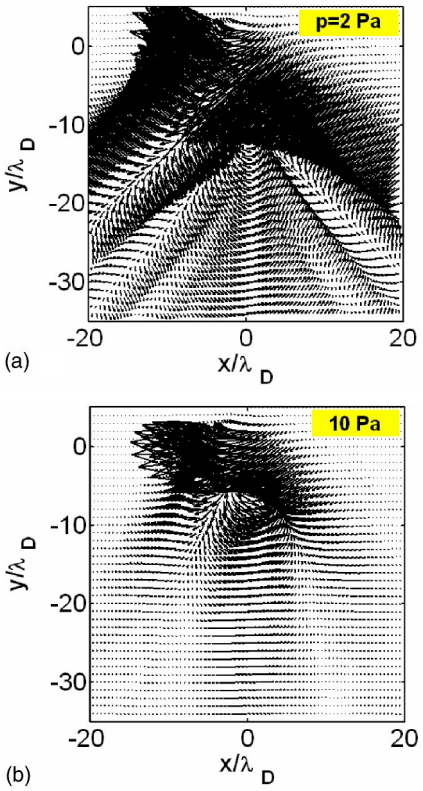

FIG. 10. The map of dust velocity field $\mathbf{u}_{d1}$ in the Mach cone region in the case of $\mathbf{v}_L \perp \mathbf{F}_L$ for discharge pressures (a) $p=2.0$ Pa and (b) $p=10$ Pa and with scanning speed kept at $M=1.1$.

distributions are shown in Fig. 10, where one sees a development of the shear-wave nature of Mach cones as the pressure increases. By comparing Fig. 10(a) with Fig. 7(a), one can see that the oscillations of the Mach wakes are greatly exaggerated in Fig. 10(a) due to weaker damping at a lower pressure. On the other hand, when comparing Fig. 10(b) with Fig. 5(b) for the $\mathbf{v}_L \| \mathbf{F}_L$ excitation, a new effect becomes apparent. One can see that the remaining single cone in Fig. 10(b) is, in fact, composed of a shear wave, whereas the cone in Fig. 5(b) is compressional. Therefore, under otherwise identical conditions, the excitation technique determines whether the nature of the Mach cone waves is shear or compressional. The effects of the pressure variation on the Mach-cone structures at subsonic scanning speeds are shown in Figs. 11 and 12. Figures 11(a) and 11(b) show the density perturbation σ_{d1}, for respectively, pressures of 2.0 Pa and 10 Pa and with $M=0.8$, and the corresponding velocity distributions are shown in Fig. 12. One can also observe in both Figs. 11 and 12 a transition from multiple compressional to single shear-wave Mach cones due to the damping effect. However, what is more important here is a transverse oscillatory wake [20] exhibited in Fig. 11(a).

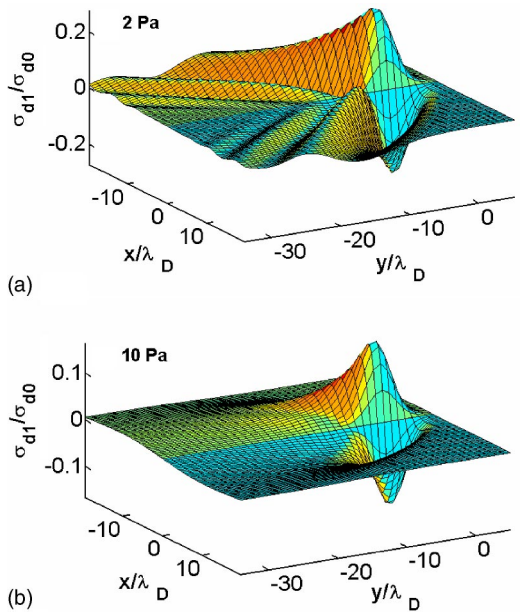

FIG. 9. The distribution of perturbed density σ_{d1} in the Mach cone region in the case of $\mathbf{v}_L \perp \mathbf{F}_L$ for discharge pressures (a) $p=2.0$ Pa and (b) $p=10$ Pa and with scanning speed kept at $M=1.1$.

IV. SUMMARY

The laser-excited Mach cones in dusty plasmas are studied by means of a 2D hydrodynamic model for a dust monolayer, which takes into account the damping effects due to the dust collisions with neutral particles. Different laser excitation techniques are investigated in accordance with recent experiments for laser-excited Mach cones. Numerical results are obtained for the density perturbation and the velocity

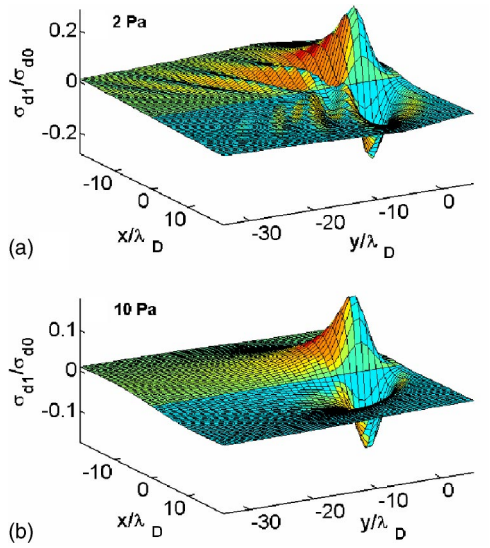

FIG. 11. The distribution of perturbed density σ_{d1} in the Mach cone region in the case of $\mathbf{v}_L \perp \mathbf{F}_L$ for discharge pressures (a) $p=2.0$ Pa and (b) $p=10$ Pa and with scanning speed kept at $M=0.8$.

distribution of the dust particles in the Mach cone region. The results obtained qualitatively agree with the previous experiments [16–20] and theory [24] for Mach cones in dusty plasmas. In particular, previously observed compressional and shear Mach cones are also reproduced here. It is found that, in the case of $\mathbf{v}_L \| \mathbf{F}_L$, the compressional Mach cones consist of multiple lateral wakes, when the scanning speed is in the supersonic range, $M>1$. When the scanning speed decreases continuously, a transition from V-shaped Mach cones to a transverse oscillatory wake can be observed.

On the other hand, in the case of $\mathbf{v}_L \perp \mathbf{F}_L$, both compressional and shear Mach cones can be achieved by adjusting the scanning speed and the discharge pressure. It is found that the compressional wave cones dominate the Mach cone region at low pressures when $M>1$, whereas a transition from the multiple compressional Mach cones to single shear-wave Mach cones can be achieved either by lowering the scanning speed or by increasing the discharge pressures.

While a surprisingly good qualitative agreement between the experiments [16–20] and the present simple 2D hydrodynamic model has been achieved, certain quantitative details are not completely reproduced in the present analytical

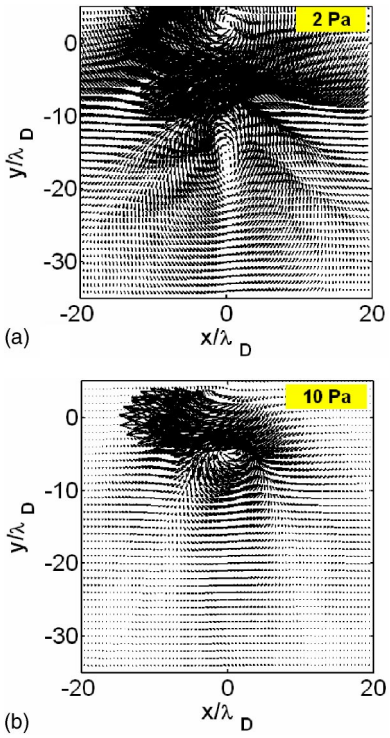

FIG. 12. The map of dust velocity field $\mathbf{u}_{d1}$ in the Mach cone region in the case of $\mathbf{v}_L \perp \mathbf{F}_L$ for discharge pressures (a) $p=2.0$ Pa and (b) $p=10$ Pa and with scanning speed kept at $M=0.8$.

theory, especially in the maps of the velocity field for the shear-wave Mach cone. Possible improvements of the present model may include adopting a more sophisticated approach, for example the quasilocalized charge approximation (QLCA) for so-called Yukawa fluid [33]. This will be our future work and this improvement will bring the details of the interaction and coupling among the dust particles into the theory, thereby extending its applicability further into the region of strong coupling.

ACKNOWLEDGMENTS

This work was jointly supported by the National Natural Science Foundation of China (No. 10275009) and by an MOEC (Ministry of Education, China) Grant for Cross-Century Excellent Scholar (Y.N.W.). Support from the Natural Sciences and Engineering Research Council of Canada is also acknowledged (Z.L.M.).

[1] Y. Hayashi and K. Tachibana, Jpn. J. Appl. Phys., Part 2 **33**, L804 (1994).
[2] J. H. Chu and L. I, Phys. Rev. Lett. **72**, 4009 (1994).
[3] H. Thomas, G. E. Morfill, V. Demmel, J. Goree, B. Feuerbacher, and D. Mohlmann, Phys. Rev. Lett. **73**, 652 (1994).
[4] A. Melzer, T. Trottenberg, and A. Piel, Phys. Lett. A **191**, 301 (1994).
[5] S. V. Vladimirov and M. Nambu, Phys. Rev. E **52**, R2172 (1995).
[6] S. V. Vladimirov and O. Ishihara, Phys. Plasmas **3**, 444 (1996).
[7] O. Ishihara and S. V. Vladimirov, Phys. Plasmas **4**, 69 (1997).
[8] G. Lapenta, Phys. Plasmas **6**, 1442 (1999).
[9] B. S. Xie, K. F. He, and Z. Q. Huang, Phys. Lett. A **253**, 83 (1999).
[10] O. Ishihara, S. V. Vladimirov, and N. F. Cramer, Phys. Rev. E **61**, 7246 (2000).
[11] G. Lapenta, Phys. Rev. E **62**, 1175 (2000).
[12] M. Lampe, G. Joyce, and G. Ganguli, Phys. Plasmas **7**, 3851 (2000).
[13] L. J. Hou, Y. N. Wang, and Z. L. Mišković, Phys. Lett. A **292**, 129 (2001).

[14] L. J. Hou, Y. N. Wang, and Z. L. Mišković, Phys. Rev. E **64**, 046406 (2001).
[15] L. J. Hou, Y. N. Wang, and Z. L. Mišković, Phys. Rev. E **68**, 016410 (2003).
[16] D. Samsonov, J. Goree, Z. W. Ma, A. Bhattacharjee, H. M. Thomas, and G. E. Morfill, Phys. Rev. Lett. **83**, 3649 (1999).
[17] D. Samsonov, J. Goree, H. M. Thomas, and G. E. Morfill, Phys. Rev. E **61**, 5557 (2000).
[18] A. Melzer, S. Nunomura, D. Samsonov, Z. W. Ma, and J. Goree, Phys. Rev. E **62**, 4162 (2000).
[19] V. Nosenko, J. Goree, Z. W. Ma, and A. Piel, Phys. Rev. Lett. **88**, 135001 (2002).
[20] V. Nosenko, J. Goree, Z. W. Ma, D. Dubin, and A. Piel, Phys. Rev. E **68**, 056409 (2003).
[21] O. Havnes, T. Aslaksen, T. W. Hartquist, F. Li, F. Melandsø, G. E. Morfill, and T. Nitter, J. Geophys. Res., [Space Phys.] **A100**, 1731 (1995).
[22] O. Havnes, F. Li, F. Melandsø, T. Aslaksen, T. W. Hartquist, G. E. Morfill, T. Nitter, and V. Tsytovich, J. Vac. Sci. Technol. A **12**, 525 (1996).
[23] O. Havnes, F. Li, T. W. Hartquist, T. Aslaksen, and A. Brattli, Planet. Space Sci. **49**, 223 (2001).
[24] D. Dubin, Phys. Plasmas **7**, 3895 (2000).
[25] A. A. Mamun, P. K. Shukla, and R. Bingham, JETP Lett. **77**, 541 (2003).
[26] P. K. Shukla, A. A. Mamun, and R. Bingham, JETP Lett. **78**, 99 (2003).
[27] P. K. Shukla and A. A. Mamun, Phys. Lett. A **315**, 258 (2003).
[28] A. A. Mamun, P. K. Shukla, and G. E. Morfill, Phys. Rev. Lett. **92**, 095005 (2004).
[29] Z. W. Ma and A. Bhattacharjee, Phys. Plasmas **9**, 3349 (2002).
[30] L. Stenflo, P. K. Shukla, and M. Y. Yu, Phys. Plasmas **7**, 2731 (2000); L. Stenflo and P. K. Shukla, *ibid.* **7**, 3472 (2000).
[31] P. Epstein, Phys. Rev. **23**, 710 (1924).
[32] F. Lado, Phys. Rev. B **17**, 2827 (1978).
[33] G. J. Kalman, P. Hartmann, Z. Donkó, and M. Rosenberg, Phys. Rev. Lett. **92**, 065001 (2004).